

# Is the protactinium(V) mono-oxo bond weaker than what we thought?<sup>†</sup>

Tamara Shaaban,<sup>a</sup> Hanna Oher,<sup>b</sup> Jean Aupiais,<sup>c</sup> Julie Champion,<sup>d</sup> André Severo Pereira Gomes,<sup>a</sup> Claire Le Naour,<sup>b</sup> Melody Maloubier,<sup>b</sup> Florent Réal,<sup>a</sup> Eric Renault,<sup>e</sup> Xavier Rocquefelte,<sup>f</sup> Bruno Siberchicot,<sup>c</sup> Valérie Vallet,<sup>a</sup> and Rémi Maurice<sup>\*f</sup>

The bond distance is the simplest and most obvious indicator of the nature of a given chemical bond. However, for rare chemistry, it may happen that it is not yet firmly established. In this communication, we will show that the formally-triple protactinium(V) mono-oxo bond is predicted longer than what was previously reported in the solid state and in solution, based on robust quantum mechanical calculations, supported by an extensive methodological study. Furthermore, additional calculations are used to demonstrate that the Pa–O<sub>oxo</sub> bond of interest is more sensitive to complexation than the supposedly analogous U–O<sub>yl</sub> ones, not only in terms of bond distance but also of finer bond descriptors associated with the effective bond multiplicity.

Protactinium (Pa,  $Z = 91$ ) is an actinide with enigmatic physico-chemical properties<sup>1,2</sup> that would differentiate the “transition-metal” like actinides (up to thorium, Th) from the heavier ones (starting with uranium, U)<sup>3</sup>. One of the key features of protactinium is its propensity to form a single oxo bond in solution in its pentavalent oxidation state<sup>4</sup>, while it is not observed for the “transition-metal” like actinides and while dioxo bonds are observed for the heavier elements such as uranium, neptunium (Np), plutonium (Pu) and americium (Am).

This single oxo bond has been characterized by X-ray absorption spectroscopy in a couple of systems<sup>5,6</sup>, in particular [PaO(C<sub>2</sub>O<sub>4</sub>)<sub>3</sub>]<sup>3-</sup> and [PaO(SO<sub>4</sub>)<sub>3</sub>]<sup>3-</sup>, with a fitted Pa–O<sub>oxo</sub> bond distance of  $\sim 1.72$  Å– $1.75$  Å, depending on the medium and conditions. The objective of the present article is to re-evaluate this bond distance from good theoretical grounds, by going well beyond our previous articles on molecular complexes that already pointed out a potential discrepancy between theory and experiment<sup>7,8</sup>. To be free of any ambiguity related to speciation in solution, we include in our study the sole solid-state compound ever reported with an occurring Pa–O<sub>oxo</sub> bond<sup>9</sup>, namely [C<sub>8</sub>H<sub>20</sub>N]<sub>2</sub>[PaOCl<sub>5</sub>]. However, we must stress that post-Hartree-Fock methods are not generally available in periodic codes, which is why we have also performed a detailed methodological study on both model and actual molecular systems (*vide infra*).

Experimental lattice parameters and bond distances are reported in Table 1. In this structure, the [PaOCl<sub>5</sub>]<sup>2-</sup> molecular unit emerges, with one shorter axial Pa–Cl<sub>ax</sub> bond distance and four longer equatorial Pa–Cl<sub>eq</sub> bond distances (non equivalent in the reported *Cc* space group), together with a Pa–O<sub>oxo</sub> bond distance

of interest of  $1.74(9)$  Å. Periodic density functional theory (DFT) calculations were performed with the VASP code<sup>10,11</sup>. Both lattice parameters and atomic positions were optimized with various setups (see Table 1). For all reported calculations, the same plane-wave energy cutoff of 550 eV was applied. From the generic PBE<sup>12</sup> calculation, the *f* levels can be effectively pushed up by an *ad hoc* Hubbard *U* term<sup>13</sup> or finer described by using a hybrid exchange-correlation functional such as PBE0<sup>14</sup>, and on top of that a (post-SCF) dispersion correction may be applied<sup>15</sup>.

It is clear that for obtaining a fair agreement between the computed and experimental lattice parameters the introduction of a dispersion correction, namely D3(BJ)<sup>15</sup>, is required (see Table 1). Once it is applied, both the PBE and PBE0 functionals yield similar lattice parameters. While the Pa–O<sub>oxo</sub> bond distance is typically increased by the +*U* correction, the introduction of Hartree-Fock exchange reduces it. Note that the dispersion correction keeps this bond distance untouched, with both the PBE and PBE0 functionals. With the more accurate PBE0 functional, we obtain a Pa–O<sub>oxo</sub> bond distance of  $1.83$  Å, which lies within the confidence interval of the experimental distance,  $1.74 \pm 0.09$  Å.

Given the computational cost and for comparison purposes, we retained the PBE+D3(BJ) method<sup>12,15</sup> for probing two well-resolved, recent, uranium structures<sup>16,17</sup>, namely (C<sub>4</sub>H<sub>12</sub>N<sub>2</sub>)[UO<sub>2</sub>Cl<sub>4</sub>] and (C<sub>4</sub>H<sub>12</sub>N<sub>2</sub>)<sub>2</sub>[UO<sub>2</sub>Cl<sub>4</sub>(H<sub>2</sub>O)]Cl<sub>2</sub>. We note that a very good agreement with experiment is observed for the lattice parameters and for the U–Cl bond distances (see Table 2), which validates the chosen level of theory. Concerning the U–O<sub>yl</sub> dioxo bond distances, we observe a standard overestimation of  $\sim 0.04$  Å to  $0.05$  Å at this level of theory. If we correct the previous PBE+D3(BJ) Pa–O<sub>oxo</sub> bond distance by the opposite amount, we obtain  $\sim 1.81$  Å to  $1.82$  Å, which again lies within the experimental confidence interval. We thus conclude at this stage that the Pa–O<sub>oxo</sub> bond distance is predicted to be slightly longer than  $1.8$  Å and thus also longer than the typical U–O<sub>yl</sub> ones.<sup>8</sup>

Without entering yet in a detailed discussion concerning the Pa–O<sub>oxo</sub> bond nature, we have performed additional periodic calculations with the PBE functional for the bare [PaO]<sup>3+</sup> and [UO<sub>2</sub>]<sup>2+</sup> systems as well as determined integrated crystal orbital bond indices (ICOBIs)<sup>18</sup> at the PBE+D3(BJ) level on the previous solid-state systems (see text below Table S1). Note that the ref-

<sup>a</sup> Univ. Lille, CNRS, UMR 8523 - PhLAM - Physique des Lasers Atomes et Molécules, F-59000 Lille, France

<sup>b</sup> Université Paris-Saclay, CNRS/IN2P3, IJCLab, 91405 Orsay, France.

<sup>c</sup> CEA, Laboratoire Matière en Conditions Extrêmes, Université Paris-Saclay, F-91680, Bruyères-le-Châtel, France; CEA, DAM, DIF, 91297 Arpajon, France

<sup>d</sup> IMT Atlantique, Nantes Université, CNRS/IN2P3, SUBATECH, F-44000 Nantes, France

<sup>e</sup> Nantes Université, CNRS, CEISAM UMR 6230, F-44000 Nantes, France

<sup>f</sup> Univ Rennes, CNRS, ISCR (Institut des Sciences Chimiques de Rennes) – UMR 6226, F-35000 Rennes, France. E-mail: remi.maurice@univ-rennes.fr

<sup>†</sup> Electronic Supplementary Information (ESI) available: Additional calculations essentially of interest for methodological purposes.

**Table 1** Optimized lattice parameters and relevant bond distances obtained for  $[\text{C}_8\text{H}_{20}\text{N}]_2[\text{PaOCl}_5]$  by periodic density functional theory calculations. Results are compared with experiment ( $Cc$  space group).

$[\text{C}_8\text{H}_{20}\text{N}]_2[\text{PaOCl}_5]$	$a$ (Å)	$b$ (Å)	$c$ (Å)	$\beta$ (°)	$d[\text{Pa}-\text{O}]$ (Å)	$d[\text{Pa}-\text{Cl}_{\text{ax}}]$ (Å)	$\bar{d}[\text{Pa}-\text{Cl}_{\text{eq}}]$ (Å) <sup>a</sup>
PBE <sup>12</sup>	14.281	14.951	13.596	91.34	1.859	2.648	2.689(6)
PBE+D3(BJ) <sup>12,15</sup>	13.301	14.840	12.745	91.65	1.859	2.624	2.673(17)
PBE+U+D3(BJ) <sup>12,13,15</sup> ( $U_{\text{eff}} = 4$ eV)	13.295	14.797	12.825	91.36	1.890	2.631	2.690(14)
PBE0 <sup>14</sup>	13.996	14.799	13.350	91.29	1.832	2.624	2.674(7)
PBE0+D3(BJ) <sup>14,15</sup>	13.153	14.665	12.518	91.59	1.832	2.608	2.659(19)
Expt. <sup>9</sup>	14.131(8)	14.218(8)	13.235(9)	91.04(3)	1.74(9)	2.42(3)	2.64(6)

<sup>a</sup>The four distances are crystallographically independent.

erence bonds in  $[\text{PaO}]^{3+}$  and  $[\text{UO}_2]^{2+}$  are both formally triple<sup>8</sup>, with a subtle distinction: in  $[\text{PaO}]^{3+}$  bonding orbitals may display mixed 6d/5f Pa characters, whereas in  $[\text{UO}_2]^{2+}$ , the 6d and 5f U characters are symmetry separated. In the bare systems, the Pa–O<sub>oxo</sub> bond is slightly longer and displays a higher ICOBI. This is also true for the  $[\text{C}_8\text{H}_{20}\text{N}]_2[\text{PaOCl}_5]$  and  $(\text{C}_4\text{H}_{12}\text{N}_2)[\text{UO}_2\text{Cl}_4]$  solid-state systems (see Figure 1). Naturally, the ICOBIs are there smaller than in the bare systems (longer distances). We note that the full crystal environment induces a lengthening of the Pa–O<sub>oxo</sub> bond by 0.037 Å, larger than that found in uranyl, 0.024 Å. This, plus the shorter Pa–Cl<sub>ax</sub> bond distance indicates that the Pa–O<sub>oxo</sub> bond is more sensitive to complexation since the *trans* position is not protected, unlike in  $[\text{UO}_2]^{2+}$  and related compounds.

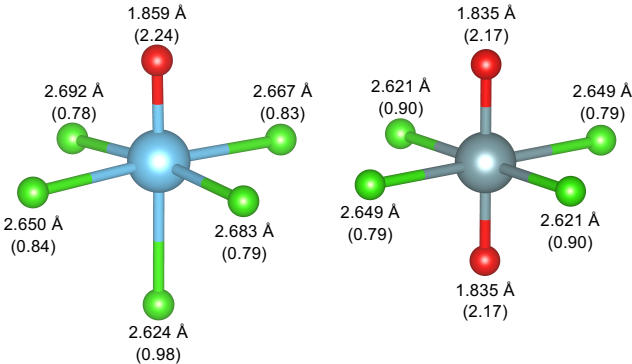


**Fig. 1** Schematic representation of the PBE+D3(BJ) atomic arrangements of the  $[\text{PaOCl}_5]^{2-}$  (left) and  $[\text{UO}_2\text{Cl}_4]^{2-}$  (right) units (visualization performed with VESTA<sup>19</sup>). The ICOBIs are given in brackets.

We now move on with complexes in solution. Static calculations, based on electronic structure theory and the application of a continuum dielectric model for solvation (implicit solvation model), lead to longer Pa–O<sub>oxo</sub> bond distances<sup>5,7</sup> than what was reported by EXAFS in solution, by  $\sim 0.10$ - $0.15$  Å, *i.e.* by more than the expected sum of the experimental and computational errors. Since this discrepancy can originate from the relative simplicity of the model used to mimic the complex in solution, we have chosen to initiate our analysis by comparing results from static quantum chemical (QC) calculations (with isolated systems) and QC molecular dynamics (MD) simulations (with systems embedded in large simulation boxes containing around 100 water molecules). Calculations and simulations were performed with the Abinit code<sup>20</sup>. For this part, we selected two prototypes:  $\text{PaOF}_3(\text{H}_2\text{O})_3$ , previously included in an *ab initio* molecular dynamics (AIMD) study<sup>21</sup>,

and the  $[\text{PaO}(\text{C}_2\text{O}_4)_3]^{3-}$  complex, previously studied by static approaches<sup>5,7</sup>. In both cases, the protactinium(V) ion displays a coordination number of 7, which practically seems to be the largest possible one in solution for this ion<sup>7,21</sup>, except in the peculiar  $[\text{PaF}_8]^{3-}$  case<sup>22</sup>.

First, we tested ten *pure* (*i.e.* nonhybrid) exchange-correlation functionals (see Table S2). For the bare  $[\text{PaO}]^{3+}$  system as well as for the isolated  $\text{PaOF}_3(\text{H}_2\text{O})_3$  and  $[\text{PaO}(\text{C}_2\text{O}_4)_3]^{3-}$  complexes, we found very homogeneous results for the Pa–O<sub>oxo</sub> bond distance of interest. Therefore, any of those ten functionals could have been used for the AIMD study. We selected the PBE functional<sup>12</sup> for the sake of homogeneity across our reported results. As can be seen in Table 3, the combined influence of the water bath and molecular dynamics has minimal impact on the Pa–O<sub>oxo</sub> bond distance. More importantly, these effects together slightly increase the bond distance (by 0.003 Å to 0.004 Å). Therefore, the previously mentioned discrepancy between theory and EXAFS on  $[\text{PaO}(\text{C}_2\text{O}_4)_3]^{3-}$  cannot be attributed to the static approach. Consequently, to facilitate a more in-depth methodological study, we will now exclusively use the static QC approach.

We have selected two protactinium(V) systems for this static study, namely  $[\text{PaO}]^{3+}$ , for obvious reasons, and  $[\text{PaO}(\text{C}_2\text{O}_4)_3]^{3-}$  as our primary case in solution. The sulfuric case<sup>6</sup> is intentionally excluded due to the unclear coordination modes of the sulfate groups (monodentate vs. bidentate fashions), though a similar issue arises for the Pa–O<sub>oxo</sub> bond distance<sup>7</sup>. Calculations were performed with three computational chemistry codes, namely Gaussian<sup>23</sup>, Molpro<sup>24</sup> and ADF<sup>25</sup>.

Since detailed results are reported in the Supporting Information (see in particular Table S3 and Table S4), we only highlight our main conclusions here. First, both employed implicit solvation models lead to a slight Pa–O<sub>oxo</sub> bond lengthening of less than 0.01 Å in the  $[\text{PaO}(\text{C}_2\text{O}_4)_3]^{3-}$  complex, which has a saturated protactinium(V) coordination sphere. Second, the spin-orbit coupling leads to an even more negligible Pa–O<sub>oxo</sub> bond lengthening. Therefore, we report either scalar or spin-orbit relativistic values for comparison purposes, but to keep things simple, we have retained scalar relativistic values in Table 4. Third, we confirm that by going from PBE<sup>12</sup> to the hybrid PBE0<sup>14</sup> functional, the Pa–O<sub>oxo</sub> bond distance is reduced by  $\sim 0.03$  Å, in accord with the already discussed solid-state results (*vide supra*). Fourth, hybrid functionals such as B3LYP<sup>26</sup> and PBE0<sup>14</sup> show good agreement with the higher level CCSD(T) method<sup>27</sup>, as does MP2<sup>28</sup>. Last, the application of a dispersion correction<sup>15</sup> is bland on the Pa–O<sub>oxo</sub> bond distance. All-in-all, we have reported the COSMO<sup>29</sup> scalar rela-

**Table 2** Optimized lattice parameters and relevant bond distances obtained for  $(\text{C}_4\text{H}_{12}\text{N}_2)[\text{UO}_2\text{Cl}_4]$  and  $(\text{C}_4\text{H}_{12}\text{N}_2)_2[\text{UO}_2\text{Cl}_4(\text{H}_2\text{O})]\text{Cl}_2$ , two representative uranyl compounds, by periodic density functional theory calculations. Results are compared with experiment (*P1* and *Pnma* space groups).

$(\text{C}_4\text{H}_{12}\text{N}_2)[\text{UO}_2\text{Cl}_4]$	<i>a</i> (Å)	<i>b</i> (Å)	<i>c</i> (Å)	$\alpha$ (°)	$\beta$ (°)	$\gamma$ (°)	<i>d</i> [U–O] (Å)	$\bar{d}$ [U–Cl] (Å) <sup><i>a</i></sup>	
PBE+D3(BJ) <sup>12,15</sup>	6.668	6.790	7.300	81.80	85.80	63.36	1.835	2.635(14)	
(dev.)	(+0.75%)	(+1.94%)	(–2.12%)	(–1.80%)	(–2.17%)	(+0.14%)			
Expt. <sup>16</sup>	6.6183(6)	6.6609(6)	7.4578(6)	83.300(3)	87.703(3)	63.273(2)	1.786(3)	2.646(9)	
$(\text{C}_4\text{H}_{12}\text{N}_2)_2[\text{UO}_2\text{Cl}_4(\text{H}_2\text{O})]\text{Cl}_2$	<i>a</i> (Å)	<i>b</i> (Å)	<i>c</i> (Å)				<i>d</i> [U–O <sub>w</sub> ] (Å)	$\bar{d}$ [U–O <sub>yl</sub> ] (Å) <sup><i>b</i></sup>	$\bar{d}$ [U–Cl] (Å) <sup><i>a</i></sup>
PBE+D3(BJ) <sup>12,15</sup>	12.172	12.418	13.409				2.513	1.8035(5)	2.768(3)
(dev.)	(–0.34%)	(–0.22%)	(–0.36%)						
Expt. <sup>17</sup>	12.2130(7)	12.4456(7)	13.4579(8)				2.499(3)	1.761(1)	2.765(3)

<sup>*a*</sup>The four distances are only crystallography equivalent two by two.

<sup>*b*</sup>The two distances are crystallography independent.

**Table 3** Joint effect of explicit solvation and molecular dynamics on the Pa–O bond distance (Å) obtained with the Abinit code<sup>20</sup> and the PBE exchange-correlation functional<sup>12</sup>.

Computational setup	PaOF <sub>3</sub> (H <sub>2</sub> O) <sub>3</sub>	[PaO(C <sub>2</sub> O <sub>4</sub> ) <sub>3</sub> ] <sup>3–</sup>
Static, isolated molecule	1.833	1.869
Dynamic (298 K), water bath, 1.5 ps	1.836	1.873

**Table 4** Scalar-relativistic An–O (An = Pa, U) bond distances obtained with the ADF code<sup>25</sup>, the COSMO implicit solvation<sup>29</sup> and the PBE0 exchange-correlation functional<sup>14</sup>, together with the corresponding delocalisation indices ( $\delta$ 's)<sup>30</sup> arising from the QTAIM<sup>31</sup> analysis.

Molecular system	<i>d</i> (Å)	$\delta$
[PaO] <sup>3+</sup>	1.710	2.33
[PaO(C <sub>2</sub> O <sub>4</sub> ) <sub>3</sub> ] <sup>3–</sup>	1.858	1.69
[UO <sub>2</sub> ] <sup>2+</sup>	1.702	2.15
[UO <sub>2</sub> Cl <sub>4</sub> ] <sup>2–</sup>	1.766	1.89
[UO <sub>2</sub> (C <sub>2</sub> O <sub>4</sub> ) <sub>3</sub> ] <sup>4–</sup>	1.7815(15)	1.84

tivistic PBE0<sup>14</sup> results in Table 4.

Before commenting on the obtained results with protactinium(V), we first assess the quality of the results obtained at the chosen level of theory based on uranyl systems, namely [UO<sub>2</sub>]<sup>2+</sup>, the well-known [UO<sub>2</sub>Cl<sub>4</sub>]<sup>2–</sup> molecular unit (already present in the  $(\text{C}_4\text{H}_{12}\text{N}_2)[\text{UO}_2\text{Cl}_4]$  solid-state system), and the [UO<sub>2</sub>(C<sub>2</sub>O<sub>4</sub>)<sub>3</sub>]<sup>4–</sup> complex. The latter has been studied both experimentally and computationally<sup>32</sup> and notably exhibits a uranium(VI) coordination number of 7, making it analogous to the [PaO(C<sub>2</sub>O<sub>4</sub>)<sub>3</sub>]<sup>3–</sup> case. As shown in Table S5, the influence of the spin-orbit coupling on the U–O<sub>yl</sub> bond distance(s) is minimal, justifying our selection of a scalar relativistic level in Table 4. Note that the PBE0 gas-phase result for [UO<sub>2</sub>]<sup>2+</sup> (1.68 Å) is in fair agreement with the reference 1.71 Å value of de Jong *et al.*<sup>33</sup>. For [UO<sub>2</sub>Cl<sub>4</sub>]<sup>2–</sup> and [UO<sub>2</sub>(C<sub>2</sub>O<sub>4</sub>)<sub>3</sub>]<sup>4–</sup>, our U–O<sub>yl</sub> bond distance values in solution of 1.77 and 1.78 Å, respectively, are furthermore of quite exceptional match with the 1.77(1) and 1.79(4) Å experimental ones<sup>32,34</sup>. Thus, we conclude that the values reported in Table 4 are of sufficient quality to allow for reliable comparisons between the protactinium(V) and uranium(VI) cases.

From Table 4, it is evident that while the An–O bond distance in the bare [PaO]<sup>3+</sup> system is slightly longer than that in [UO<sub>2</sub>]<sup>2+</sup>, it is much longer in [PaO(C<sub>2</sub>O<sub>4</sub>)<sub>3</sub>]<sup>3–</sup> than in [UO<sub>2</sub>Cl<sub>4</sub>]<sup>2–</sup> and [UO<sub>2</sub>(C<sub>2</sub>O<sub>4</sub>)<sub>3</sub>]<sup>4–</sup>. In other words, even if [PaO]<sup>3+</sup> may be seen as a “half” [UO<sub>2</sub>]<sup>2+</sup> unit, the coordination-induced bond lengthening is much more pronounced in the case of protactinium(V) (*ca.* 0.15 Å) than in the uranium(VI) one (*ca.* 0.07 Å), being in

practice doubled. Thus, we definitely conclude that [PaO]<sup>3+</sup> exhibits a much stronger sensitivity to extra coordination compared to [UO<sub>2</sub>]<sup>2+</sup>.

To further check if this perspective on bond distance corroborates with the bonding perspective, we have also determined delocalisation indices ( $\delta$ 's)<sup>30</sup> within the QTAIM framework<sup>31</sup> (other indicators are given in Table S6). We recall that  $\delta$  values, by definition, correspond to the number of electron pairs shared between two atoms, reflecting the effective bond multiplicity. In the bare [UO<sub>2</sub>]<sup>2+</sup> system, six bonding orbitals of  $\sigma_{u,g}$  and  $\pi_{u,g}$  are doubly occupied in the ground state<sup>35</sup>, the *ungerade* ones involving 5f orbitals of U and the *gerade* ones involving 6d orbitals of U. Thus, the U–O<sub>yl</sub> bonds are formally triple bonds. As shown in Table 4,  $\delta$  in there much smaller than 3, which is due to the strong asymmetry of those bonds (“polar” character<sup>36</sup>). Upon complexation,  $\delta$  is reduced by  $\sim 0.3$  in both [UO<sub>2</sub>Cl<sub>4</sub>]<sup>2–</sup> and [UO<sub>2</sub>(C<sub>2</sub>O<sub>4</sub>)<sub>3</sub>]<sup>4–</sup>. Note that our 1.89 value for [UO<sub>2</sub>Cl<sub>4</sub>]<sup>2–</sup> is consistent with the 1.87 one of Wellington *et al.*<sup>36</sup>.

In the bare [PaO]<sup>3+</sup> system, three bonding orbitals are populated in the ground state. Note that due to the absence of a symmetry center, the 5f and 6d orbitals of Pa are not symmetry separated anymore. The obtained  $\delta$  value, 2.33, is slightly higher than in [UO<sub>2</sub>]<sup>2+</sup>, which is 2.15. This means that the slightly longer Pa–O<sub>oxo</sub> bond distance goes together with a slightly more covalent Pa–O<sub>oxo</sub> bond in [PaO]<sup>3+</sup> compared to the U–O<sub>yl</sub> ones in [UO<sub>2</sub>]<sup>2+</sup>. This is attributed to the smaller formal charge of protactinium(V) *versus* uranium(VI), hence a larger ionic radius. After complexation,  $\delta$  is reduced by  $\sim 0.6$  in [PaO(C<sub>2</sub>O<sub>4</sub>)<sub>3</sub>]<sup>3–</sup>. It is interesting to note that the observed factor of 2 in the complexation-induced bond lengthening perfectly correlates with the factor of 2 reduction in  $\delta$ . Thus, these two bond descriptors point toward the exact same conclusion.

In this article, we have shown that the Pa–O<sub>oxo</sub> bond is more sensitive to complexation than the U–O<sub>yl</sub> ones. We attribute this to the fact that the *trans* position is not protected in the [PaO]<sup>3+</sup> chemical moiety. This leaves room for coordination with specific bonding at this position in real chemical systems. For instance, it can occur in the solid-state [PaOCl<sub>5</sub>]<sup>2–</sup> molecular unit (see Tables S7, S8 and S9 and the associated discussion on bonding) or in the [PaO(C<sub>2</sub>O<sub>4</sub>)<sub>3</sub>]<sup>3–</sup> complex. Specifically, the distance to the *trans* ligands is expected to be shorter than to the *cis* ones due to the inverse *trans* effect already observed and analyzed in actinide complexes<sup>37–41</sup>. Since the Pa–O<sub>oxo</sub> bond distance is predicted to be longer than the U–O<sub>yl</sub> one, the previous experimentally re-

ported Pa–O<sub>oxo</sub> bond distances must be revised. According to all of our calculations, this bond distance is in any case predicted to be slightly longer than 1.8 Å, indicating that it is weaker than previously thought. An obvious perspective of this work would consist in performing new experiments to confirm these findings. Furthermore, this work is already a key step in the exploration of the intriguing physico-chemical properties of the actinides since it confirms the peculiarity of protactinium, which definitely qualifies it as a trend separator within the actinide series.

## Author Contributions

This article is the result of a collective effort supported by the ANR CHES project (contract No. ANR-21-CE29-0027). T.S. is the primary contributor for the performed calculations, completed by additional work by H.O., X.R. and B.S. The first draft was written by R.M. and each version was approved by all the co-authors.

## Data availability

The data supporting this article have been included as part of the Supplementary Information<sup>†</sup> and the optimized structures can be accessed at the Zenodo repository via the following DOI: 10.5281/zenodo.13494221.

## Conflicts of interest

There are no conflicts to declare.

## Notes and references

- D. Brown and A. G. Maddock, *Q. Rev. Chem. Soc.*, 1963, **17**, 289–341.
- R. Wilson, *Nat. Chem.*, 2012, **4**, 586.
- R. E. Wilson, S. De Sio and V. Vallet, *Nat. Commun.*, 2018, **9**, 1–9.
- C. Le Naour, M. Maloubier and J. Aupiais, *Radiochim. Acta*, 2022, **110**, 481–493.
- M. Mendes, S. Hamadi, C. Le Naour, J. Roques, A. Jeanson, C. Den Auwer, P. Moisy, S. Topin, J. Aupiais, C. Hennig and M. V. Di Giandomenico, *Inorg. Chem.*, 2010, **49**, 9962–9971.
- C. Le Naour, D. Trubert, M. V. Di Giandomenico, C. Fillaux, C. Den Auwer, P. Moisy and C. Hennig, *Inorg. Chem.*, 2005, **44**, 9542–9546.
- H. Oher, J. Delafoulhouze, E. Renault, V. Vallet and R. Maurice, *Phys. Chem. Chem. Phys.*, 2023, **25**, 10033–10041.
- T. Shaaban, F. Réal, R. Maurice and V. Vallet, *Chem. Eur. J.*, 2024, **30**, e202304068.
- D. Brown, C. T. Reynolds and P. T. Moseley, *J. Chem. Soc., Dalton Trans.*, 1972, 857–859.
- G. Kresse and J. Hafner, *Phys. Rev. B*, 1993, **47**, 558–561.
- G. Kresse and D. Joubert, *Phys. Rev. B*, 1999, **59**, 1758–1775.
- J. P. Perdew, K. Burke and M. Ernzerhof, *Phys. Rev. Lett.*, 1997, **78**, 1396–1396.
- S. L. Dudarev, G. A. Botton, S. Y. Savrasov, C. J. Humphreys and A. P. Sutton, *Phys. Rev. B*, 1998, **57**, 1505–1509.
- C. Adamo, G. E. Scuseria and V. Barone, *J. Chem. Phys.*, 1999, **111**, 2889–2899.
- S. Grimme, S. Ehrlich and L. Goerigk, *J. Comput. Chem.*, 2011, **32**, 1456–1465.
- H. Rajapaksha, L. J. Augustine, S. E. Mason and T. Z. Forbes, *Angew. Chem. Int. Ed.*, 2023, **62**, e202305073.
- H. Rajapaksha, S. E. Mason and T. Z. Forbes, *Inorg. Chem.*, 2023, **62**, 14318–14325.
- P. C. Müller, C. Ertural, J. Hempelmann and R. Dronskowski, *J. Phys. Chem. C*, 2021, **125**, 7959–7970.
- K. Momma and F. Izumi, *J. Appl. Crystallogr.*, 2008, **41**, 653–658.
- X. Gonze, B. Amadon, G. Antonius, F. Arnardi, L. Baguet, J.-M. Beuken, J. Bieder, F. Bottin, J. Bouchet, E. Bousquet, N. Brouwer, F. Bruneval, G. Brunin, T. Cavignac, J.-B. Charraud, W. Chen, M. Côté, S. Cottenier, J. Denier, G. Geneste, P. Ghosez, M. Giantomassi, Y. Gillet, O. Gingras, D. R. Hamann, G. Hautier, X. He, N. Helbig, N. Holzwarth, Y. Jia, F. Jollet, W. Lafargue-Dit-Hauret, K. Lejaeghere, M. A. Marques, A. Martin, C. Martins, H. P. Miranda, F. Naccarato, K. Persson, G. Petretto, V. Planes, Y. Pouillon, S. Prokhorenko, F. Ricci, G.-M. Rignanese, A. H. Romero, M. M. Schmitt, M. Torrent, M. J. van Setten, B. Van Troeye, M. J. Verstraete, G. Zérah and J. W. Zwanziger, *Comput. Phys. Commun.*, 2020, **248**, 107042.
- B. Siberchicot, J. Aupiais and C. L. Naour, *Radiochim. Acta*, 2021, **109**, 673–680.
- M. Bukhsh, J. Flegelheimer, F. Hall, A. Maddock and C. de Miranda, *J. Inorg. Nucl. Chem.*, 1966, **28**, 421–431.
- M. J. Frisch, G. W. Trucks, H. B. Schlegel, G. E. Scuseria, M. A. Robb, J. R. Cheeseman, G. Scalmani, V. Barone, G. A. Petersson, H. Nakatsuji, X. Li, M. Caricato, A. V. Marenich, J. Bloino, B. G. Janesko, R. Gomperts, B. Mennucci, H. P. Hratchian, J. V. Ortiz, A. F. Izmaylov, J. L. Sonnenberg, D. Williams-Young, F. Ding, F. Lipparini, F. Egidi, J. Goings, B. Peng, A. Petrone, T. Henderson, D. Ranasinghe, V. G. Zakrzewski, J. Gao, N. Rega, G. Zheng, W. Liang, M. Hada, M. Ehara, K. Toyota, R. Fukuda, J. Hasegawa, M. Ishida, T. Nakajima, Y. Honda, O. Kitao, H. Nakai, T. Vreven, K. Throssell, J. A. Montgomery, Jr., J. E. Peralta, F. Ogliaro, M. J. Bearpark, J. J. Heyd, E. N. Brothers, K. N. Kudin, V. N. Staroverov, T. A. Keith, R. Kobayashi, J. Normand, K. Raghavachari, A. P. Rendell, J. C. Burant, S. S. Iyengar, J. Tomasi, M. Cossi, J. M. Millam, M. Klene, C. Adamo, R. Cammi, J. W. Ochterski, R. L. Martin, K. Morokuma, O. Farkas, J. B. Foresman and D. J. Fox, *Gaussian~16 Revision C.01*, 2016, Gaussian Inc. Wallingford CT.
- H.-J. Werner, P. J. Knowles, G. Knizia, F. R. Manby, M. Schütz, P. Celani, W. Gyröffy, D. Kats, T. Korona, R. Lindh, A. Mitrushenkov, G. Rauhut, K. R. Shamasundar, T. B. Adler, R. D. Amos, S. J. Bennie, A. Bernhardsson, A. Berning, D. L. Cooper, M. J. O. Deegan, A. J. Dobyn, F. Eckert, E. Goll, C. Hampel, A. Hesselmann, G. Hetzer, T. Hrenar, G. Jansen, C. Köppl, S. J. R. Lee, Y. Liu, A. W. Lloyd, Q. Ma, R. A. Mata, A. J. May, S. J. McNicholas, W. Meyer, T. F. Miller III, M. E. Mura, A. Nicklass, D. P. O'Neill, P. Palmieri, D. Peng, K. Pflüger, R. Pitzer, M. Reiher, T. Shiozaki, H. Stoll, A. J. Stone, R. Tarroni, T. Thorsteinsson, M. Wang and M. Welborn, *MOLPRO, a package of ab initio programs, version 2023.2*.
- G. te Velde, F. M. Bickelhaupt, E. J. Baerends, C. Fonseca Guerra, S. J. A. van Gisbergen, J. G. Snijders and T. Ziegler, *J. Comput. Chem.*, 2001, **22**, 931–967.
- P. J. Stephens, F. J. Devlin, C. F. Chabalowski and M. J. Frisch, *J. Chem. Phys.*, 1994, **98**, 11623–11627.
- I. Purvis, George D. and R. J. Bartlett, *J. Chem. Phys.*, 1982, **76**, 1910–1918.
- C. Möller and M. S. Plesset, *Phys. Rev.*, 1934, **46**, 618–622.
- C. C. Pye and T. Ziegler, *Theor. Chem. Acc.*, 1999, **101**, 396–408.
- C. Outeiral, M. A. Vincent, A. Martín Pendás and P. L. A. Popelier, *Chem. Sci.*, 2018, **9**, 5517–5529.
- R. F. W. Bader, *Chem. Rev.*, 1991, **91**, 893–928.
- V. Vallet, H. Moll, U. Wahlgren, Z. Szabó and I. Grenthe, *Inorg. Chem.*, 2003, **42**, 8598–8598.
- W. A. de Jong, L. Visscher and W. C. Nieuwpoort, *J. Mol. Struct. THEOCHEM*, 1999, **458**, 41–52.
- K. Servaes, C. Hennig, R. Van Deun and C. Görlner-Walrand, *Inorg. Chem.*, 2005, **44**, 7705–7707.
- R. G. Denning, *J. Phys. Chem. A*, 2007, **111**, 4125–4143.
- J. P. Wellington, A. Kerridge and N. Kaltsoyannis, *Polyhedron*, 2016, **116**, 57–63.
- V. Pershina, *Radiochim. Acta*, 1999, **84**, 79–84.
- V. Pershina, *Radiochim. Acta*, 1998, **80**, 65–73.
- E. O'Grady and N. Kaltsoyannis, *J. Chem. Soc., Dalton Trans.*, 2002, 1233–1239.
- I. Fryer-Kanssen and A. Kerridge, *Chem. Commun.*, 2018, **54**, 9761–9764.
- L. C. Motta and J. Autschbach, *Nat. Chem.*, 2023, **14**, 4307.

# Supporting Information:

## Is the protactinium(V) mono-oxo bond weaker than what we thought?

Tamara Shaaban,<sup>†</sup> Hanna Oher,<sup>‡</sup> Jean Aupiais,<sup>¶</sup> Julie Champion,<sup>§</sup> André Severo Peirera Gomes,<sup>†</sup> Claire Le Naour,<sup>‡</sup> Melody Maloubier,<sup>‡</sup> Florent Réal,<sup>†</sup> Eric Renault,<sup>||</sup> Xavier Rocquefelte,<sup>⊥</sup> Bruno Siberchicot,<sup>¶</sup> Valérie Vallet,<sup>†</sup> and Rémi Maurice<sup>\*,⊥</sup>

<sup>†</sup>*Univ. Lille, CNRS, UMR 8523 - PhLAM - Physique des Lasers Atomes et Molécules, F-59000 Lille, France*

<sup>‡</sup>*Université Paris-Saclay, CNRS/IN2P3, IJCLab, 91405 Orsay, France*

<sup>¶</sup>*CEA, Laboratoire Matière en Conditions Extrêmes, Université Paris-Saclay, F-91680, Bruyères-le-Châtel, France; CEA, DAM, DIF, 91297 Arpajon, France*

<sup>§</sup>*IMT Atlantique, Nantes Université, CNRS/IN2P3, SUBATECH, F-44000 Nantes, France*

<sup>||</sup>*Nantes Université, CNRS, CEISAM UMR 6230, F-44000 Nantes, France*

<sup>⊥</sup>*Univ Rennes, CNRS, ISCR (Institut des Sciences Chimiques de Rennes) – UMR 6226, F-35000 Rennes, France*

E-mail: remi.maurice@univ-rennes.fr

# List of Tables

S1	Integrated crystal orbital bond indices (ICOBIs) <sup>S1</sup> obtained at the optimized structures (see Tables 1 and 2). Mean values are reported when related bonds are crystallography independent. . . . .	S-4
S2	Benchmark of ten exchange-correlation (XC) functionals based on the Abinit code <sup>S2</sup> for selected protactinium molecular systems. Only the Pa–O bond distance (Å) is reported. . . . .	S-5
S3	Role of implicit solvation (C-PCM <sup>S3</sup> ) on the Pa–O bond distance (Å) obtained with Gaussian <sup>S4</sup> and the default radii (UFF <sup>S5</sup> ). . . . .	S-6
S4	Role of implicit solvation (COSMO <sup>S6</sup> ) on the Pa–O bond distance (Å) obtained with ADF <sup>S7</sup> and the default radii. <sup>S8</sup> The ZORA <sup>S9</sup> Hamiltonian was used. Values in red are reported from the main text for convenience. . . . .	S-7
S5	Role of implicit solvation (COSMO <sup>S6</sup> ) on the U–O bond distance(s) (Å) obtained with ADF <sup>S7</sup> and the default radii. The ZORA <sup>S9</sup> Hamiltonian was used. Values in red are reported from the main text for convenience. . . . .	S-8
S6	QTAIM bonding indicators obtained at the An–O (An = Pa, U) bond critical points and Bader charges, based on ADF <sup>S7</sup> calculations with the COSMO implicit solvation <sup>S6</sup> and the PBE0 exchange-correlation functional. <sup>S10</sup> Distances and delocalisation indices are reported from the main text for convenience. . . . .	S-9
S7	Mayer <sup>S11</sup> and Wiberg <sup>S12</sup> bond indices of the Pa–O and Pa–Cl bonds within the [PaO(Cl) <sub>5</sub> ] <sup>2-</sup> cluster, at the PBE+D3(BJ) solid-state geometry. Calculations were performed with ADF <sup>S7</sup> and the TZ2P basis sets. <sup>S13</sup> . . . . .	S-10
S8	Pa (5f and 6d orbitals) and O atomic orbital contributions to the $\sigma$ and $\pi$ Pa–O natural localized molecular orbitals (NLMOs) <sup>S14</sup> within [PaO(Cl) <sub>5</sub> ] <sup>2-</sup> cluster (same computational details as in Table S7). . . . .	S-10

S9 Pa (5f and 6d orbitals) and Cl atomic orbital contributions to the  $\sigma$  and  $\pi$   
Pa–Cl natural localized molecular orbitals (NLMOs)<sup>S14</sup> within  $[\text{PaO}(\text{Cl})_5]^{2-}$   
cluster (same computational details as in Table S7). . . . . S-10

Table S1: Integrated crystal orbital bond indices (ICOBIs)<sup>S1</sup> obtained at the optimized structures (see Tables 1 and 2). Mean values are reported when related bonds are crystallography independent.

$[\text{C}_8\text{H}_{20}\text{N}]_2[\text{PaOCl}_5]$	Pa–O	Pa–Cl <sub>ax</sub>	Pa–Cl <sub>eq</sub>
PBE+D3(BJ)	2.24	0.98	0.81
$(\text{C}_4\text{H}_{12}\text{N}_2)[\text{UO}_2\text{Cl}_4]$	U–O <sub>yl</sub>		U–Cl
PBE+D3(BJ)	2.17		0.85
$(\text{C}_4\text{H}_{12}\text{N}_2)_2[\text{UO}_2\text{Cl}_4(\text{H}_2\text{O})]\text{Cl}_2$	U–O <sub>yl</sub>	U–O <sub>w</sub>	U–Cl
PBE+D3(BJ)	2.32	0.36	0.63

For assessing the impact of the “environment”, bare  $[\text{PaO}]^{3+}$  and  $[\text{UO}_2]^{2+}$  systems have been optimized at the PBE level within large cubic boxes, ensuring more than 10 Å of distance between two molecular units. The resulting bond distances were 1.822 and 1.811 Å, respectively, together with ICOBIs of 2.97 and 2.66. These values serve as references to assess the impact of coordination in the crystal structures on the bonding of the  $[\text{PaO}]^{3+}$  and  $[\text{UO}_2]^{2+}$  subunits. This impact on bonding, referred to as  $\Delta\text{ICOBI}$ , was found to be  $-0.73$  for  $[\text{PaO}]^{3+}$  in  $[\text{C}_8\text{H}_{20}\text{N}]_2[\text{PaOCl}_5]$  and  $-0.49$  and  $-0.34$  in  $(\text{C}_4\text{H}_{12}\text{N}_2)[\text{UO}_2\text{Cl}_4]$  and  $(\text{C}_4\text{H}_{12}\text{N}_2)_2[\text{UO}_2\text{Cl}_4(\text{H}_2\text{O})]\text{Cl}_2$ , respectively.

Note that the ICOBI is larger in  $(\text{C}_4\text{H}_{12}\text{N}_2)_2[\text{UO}_2\text{Cl}_4(\text{H}_2\text{O})]\text{Cl}_2$  than in  $(\text{C}_4\text{H}_{12}\text{N}_2)[\text{UO}_2\text{Cl}_4]$  by 0.15, corroborating the water-induced effective bond reinforcement observed by Rajapaksha et al.<sup>S15</sup>. This bond reinforcement is concomitant with a reduction of the U–Cl ICOBI, meaning that it is in fact indirect: by weakening the in-plane bonds with water addition, the uranyl bonds are effectively less destabilized, thus appearing reinforced.

Note that the valence 7p levels of Pa and U are omitted from the ICOBI analysis by absence of such basis functions in the used program<sup>S16</sup> (the procedure requires projection of the plane waves onto a localized basis). Since these atomic levels only have a limited impact on bonding, their omission does not significantly affect our analysis.



Table S2: Benchmark of ten exchange-correlation (XC) functionals based on the Abinit code<sup>S2</sup> for selected protactinium molecular systems. Only the Pa–O bond distance (Å) is reported.

XC functional	[PaO] <sup>3+</sup>	PaOF <sub>3</sub> (H <sub>2</sub> O) <sub>3</sub>	[PaO(C <sub>2</sub> O <sub>4</sub> ) <sub>3</sub> ] <sup>3-</sup>
PW91 <sup>S17</sup>	1.710	1.817	1.851
LDA (Wigner) <sup>S18</sup>	1.723	1.832	1.867
PBE <sup>S19</sup>	1.722	1.833	1.869
HTCH93 <sup>S20</sup>	1.710	1.813	1.842
HTCH120 <sup>S21</sup>	1.710	1.814	1.847
HTCH147 <sup>S21</sup>	1.710	1.813	1.845
HTCH407 <sup>S22</sup>	1.708	1.811	1.848
GGA (Wu) <sup>S23</sup>	1.715	1.824	1.860
HTBS <sup>S24</sup>	1.743	1.865	1.887
MOHLYP <sup>S25</sup>	1.730	1.842	1.874

Table S3: Role of implicit solvation (C-PCM<sup>S3</sup>) on the Pa–O bond distance (Å) obtained with Gaussian<sup>S4</sup> and the default radii (UFF<sup>S5</sup>).

[PaO] <sup>3+</sup>	Gas phase	C-PCM
B3PW91 <sup>S26</sup>	1.689	1.759
B3LYP <sup>S27</sup>	1.697	1.771
PBE <sup>S19</sup>	1.717	1.782
PBE0 <sup>S10</sup>	1.681	1.752
PBE0+D3(BJ) <sup>S10,S28</sup>	1.681	1.752
MP2 <sup>S29</sup>	1.714	1.766

[PaO(C <sub>2</sub> O <sub>4</sub> ) <sub>3</sub> ] <sup>3-</sup>	Gas phase	C-PCM
B3PW91 <sup>S26</sup>	1.850	1.856
B3LYP <sup>S27</sup>	1.862	1.867
PBE <sup>S19</sup>	1.874	1.881
PBE0 <sup>S10</sup>	1.843	1.849
PBE0+D3(BJ) <sup>S10,S28</sup>	1.844	1.849
MP2 <sup>S29</sup>	1.857	1.857

The def2-TZVP basis sets<sup>S30</sup> were used on all atoms except for Pa, which was treated with the ECP60MWB energy-consistent pseudopotential<sup>S31</sup> along with its corresponding segmented basis set.<sup>S32</sup> Overall, a bond lengthening of  $\sim 0.07$  Å is observed for [PaO]<sup>3+</sup> and  $\sim 0.006$  Å for [PaO(C<sub>2</sub>O<sub>4</sub>)<sub>3</sub>]<sup>3-</sup>, respectively. Notably, there was minimal variation when changing the underlying electronic structure theory method.

Additionally, calculations were conducted in the gas phase using Molpro,<sup>S33</sup> yielding a scalar-relativistic CCSD(T)<sup>S34</sup> value of 1.703 Å for [PaO]<sup>3+</sup>. The MP2 and B3LYP calculations were also repeated for cross-checking, leading with this setup to 1.714 and 1.698 Å, respectively; values which are identical to those obtained using the Gaussian software.

Table S4: Role of implicit solvation (COSMO<sup>S6</sup>) on the Pa–O bond distance (Å) obtained with ADF<sup>S7</sup> and the default radii.<sup>S8</sup> The ZORA<sup>S9</sup> Hamiltonian was used. Values in red are reported from the main text for convenience.

$[\text{PaO}]^{3+}$	Relativity	Gas phase	COSMO
B3LYP <sup>S27</sup>	Scalar	1.705	1.729
	Spin-orbit	1.707	1.731
PBE0 <sup>S10</sup>	Scalar	1.688	1.710
	Spin-orbit	1.690	1.713

$[\text{PaO}(\text{C}_2\text{O}_4)_3]^{3-}$	Relativity	Gas phase	COSMO
B3LYP <sup>S27</sup>	Scalar	1.871	1.878
	Spin-orbit	1.873	1.881
PBE0 <sup>S10</sup>	Scalar	1.852	1.858
	Spin-orbit	1.854	1.862

The TZ2P basis sets<sup>S13</sup> were used on all atoms. By comparing Table S3 and Table S4, it is clear that the COSMO model leads to a lesser impact of solvation on the Pa-O bond distance than the C-PCM one. Test calculations have shown that this is essentially due to the use of the default UFF radii (rescaled by the 1.1 default  $\alpha$  value). Despite this moderate discrepancy, the previous trend holds (solvation-induced bond lengthening).

Table S5: Role of implicit solvation (COSMO<sup>S6</sup>) on the U–O bond distance(s) (Å) obtained with ADF<sup>S7</sup> and the default radii. The ZORA<sup>S9</sup> Hamiltonian was used. Values in red are reported from the main text for convenience.

$[\text{UO}_2]^{2+}$	Relativity	Gas phase	COSMO
PBE0 <sup>S10</sup>	Scalar	1.684	<b>1.702</b>
	Spin-orbit	1.687	1.705
$[\text{UO}_2\text{Cl}_4]^{2-}$	Relativity	Gas phase	COSMO
PBE0 <sup>S10</sup>	Scalar	1.763	<b>1.766</b>
	Spin-orbit	1.767	1.771
$[\text{UO}_2(\text{C}_2\text{O}_4)_3]^{4-}$	Relativity	Gas phase	COSMO
PBE0 <sup>S10</sup>	Scalar	1.779(3)	<b>1.7815(15)</b>
	Spin-orbit	1.783(3)	1.786(2)

The TZ2P basis sets<sup>S13</sup> were used on all atoms. As other deviation values reported in parenthesis in the main text for mean distances, the standard deviations have been computed using the following formula:

$$\sigma = \sqrt{\frac{1}{N} \sum_{i=1}^N (d_i - \bar{d})^2} \quad (1)$$

where  $N$  is the number of distances entering the calculation of the mean  $\bar{d}$  value. In other words, no Bessel’s correction was applied.

Table S6: QTAIM bonding indicators obtained at the An–O (An = Pa, U) bond critical points and Bader charges, based on ADF<sup>S7</sup> calculations with the COSMO implicit solvation<sup>S6</sup> and the PBE0 exchange-correlation functional.<sup>S10</sup> Distances and delocalisation indices are reported from the main text for convenience.

System	$d$ (Å)	$\rho$ , a.u.	$\nabla^2\rho$	G, a.u.	V, a.u.	$ V /G$	H, a.u.	$q(\text{An})$ , a.u.	$q(\text{X})$ , a.u.	$\delta$
$[\text{PaO}]^{3+}$	1.710	0.36	0.33	0.58	-1.07	1.84	-0.50	3.69	-0.69	2.33
$[\text{PaO}(\text{C}_2\text{O}_4)_3]^{3-}$	1.858	0.25	0.36	0.34	-0.59	1.74	-0.25	3.09	-1.14	1.69
$[\text{UO}_2]^{2+}$	1.702	0.36	0.39	0.59	-1.10	1.86	-0.49	3.53	-0.77	2.15
$[\text{UO}_2\text{Cl}_4]^{2-}$	1.766	0.30	0.36	0.46	-0.83	1.80	-0.37	2.93	-0.97	1.89
$[\text{UO}_2(\text{C}_2\text{O}_4)_3]^{4-}$	1.7815(15)	0.29	0.36	0.44	-0.79	1.80	-0.35	2.41	-0.73	1.84

Table S7: Mayer<sup>S11</sup> and Wiberg<sup>S12</sup> bond indices of the Pa–O and Pa–Cl bonds within the  $[\text{PaO}(\text{Cl})_5]^{2-}$  cluster, at the PBE+D3(BJ) solid-state geometry. Calculations were performed with ADF<sup>S7</sup> and the TZ2P basis sets.<sup>S13</sup>

	Pa–O	Pa–Cl <sub>ax</sub>	Pa–Cl <sub>eq</sub>
Mayer	2.02	0.91	0.79
Wiberg	2.07	1.03	0.91

Table S8: Pa (5f and 6d orbitals) and O atomic orbital contributions to the  $\sigma$  and  $\pi$  Pa–O natural localized molecular orbitals (NLMOs)<sup>S14</sup> within  $[\text{PaO}(\text{Cl})_5]^{2-}$  cluster (same computational details as in Table S7).

$\sigma$			$\pi$		
Pa(5f)	Pa(6d)	O(s/p)	Pa(5f)	Pa(6d)	O(s/p)
16.2	6.4	76.4	10.7	9.3	79.7

Table S9: Pa (5f and 6d orbitals) and Cl atomic orbital contributions to the  $\sigma$  and  $\pi$  Pa–Cl natural localized molecular orbitals (NLMOs)<sup>S14</sup> within  $[\text{PaO}(\text{Cl})_5]^{2-}$  cluster (same computational details as in Table S7).

	$\sigma$			$\pi$		
	Pa(5f)	Pa(6d)	Cl(s/p)	Pa(5f)	Pa(6d)	Cl(s/p)
Cl <sub>ax</sub>	8.1	6.2	83.5	3.7	3.9	92.2
Cl <sub>eq</sub>	4.7	7.2	85.3			

To cross-check our previous analysis of the solid-state  $[\text{C}_8\text{H}_{20}\text{N}]_2[\text{PaOCl}_5]$  compound based on ICOBIs (see Table S1 and the related discussion), we have also performed bonding analyses within the molecular quantum chemistry framework, based on the  $[\text{PaO}(\text{Cl})_5]^{2-}$  cluster, defined at the solid-state geometry. Clearly, the deviation to the ideal triple bond is confirmed with both the Mayer<sup>S11</sup> and Wiberg<sup>S12</sup> bond indices and the specificity of the Pa–Cl<sub>ax</sub> bond is also reproduced. We have also computed atomic contributions per shell to the  $\sigma$  and  $\pi$  bonds between the atoms of interest, when applicable (see Tables S8 and S9). While both the Pa–O and Pa–Cl<sub>ax</sub> bonds display actual  $\pi$  character, it is absent from the Pa–Cl<sub>eq</sub> bonds. This, together with the shorter Pa–Cl<sub>eq</sub> bond distance (compared to the Pa–Cl<sub>ax</sub> ones), is in fact a signature for the inverse *trans* effect, expected for  $[\text{C}_8\text{H}_{20}\text{N}]_2[\text{PaOCl}_5]$ .<sup>S35</sup>

## References

- (S1) Müller, P. C.; Ertural, C.; Hempelmann, J.; Dronskowski, R. Crystal Orbital Bond Index: Covalent Bond Orders in Solids. *J. Phys. Chem. C* **2021**, *125*, 7959–7970, DOI: 10.1021/acs.jpcc.1c00718.
- (S2) Gonze, X.; Amadon, B.; Antonius, G.; Arnardi, F.; Baguet, L.; Beuken, J.-M.; Bieder, J.; Bottin, F.; Bouchet, J.; Bousquet, E.; Brouwer, N.; Bruneval, F.; Brunin, G.; Cavignac, T.; Charraud, J.-B.; Chen, W.; Côté, M.; Cottenier, S.; Denier, J.; Geneste, G.; Ghosez, P.; Giantomassi, M.; Gillet, Y.; Gingras, O.; Hamann, D. R.; Hautier, G.; He, X.; Helbig, N.; Holzwarth, N.; Jia, Y.; Jollet, F.; Lafargue-Dit-Hauret, W.; Lejaeghere, K.; Marques, M. A.; Martin, A.; Martins, C.; Miranda, H. P.; Naccarato, F.; Persson, K.; Petretto, G.; Planes, V.; Pouillon, Y.; Prokhorenko, S.; Ricci, F.; Rignanese, G.-M.; Romero, A. H.; Schmitt, M. M.; Torrent, M.; van Setten, M. J.; Van Troeye, B.; Verstraete, M. J.; Zérah, G.; Zwanziger, J. W. The Abinit project: Impact, environment and recent developments. *Comput. Phys. Commun.* **2020**, *248*, 107042, DOI: 10.1016/j.cpc.2019.107042.
- (S3) Cossi, M.; Rega, N.; Scalmani, G.; Barone, V. Energies, structures, and electronic properties of molecules in solution with the C-PCM solvation model. *J. Comput. Chem.* **2003**, *24*, 669–681, DOI: 10.1002/jcc.10189.
- (S4) Frisch, M. J.; Trucks, G. W.; Schlegel, H. B.; Scuseria, G. E.; Robb, M. A.; Cheeseman, J. R.; Scalmani, G.; Barone, V.; Petersson, G. A.; Nakatsuji, H.; Li, X.; Caricato, M.; Marenich, A. V.; Bloino, J.; Janesko, B. G.; Gomperts, R.; Menucci, B.; Hratchian, H. P.; Ortiz, J. V.; Izmaylov, A. F.; Sonnenberg, J. L.; Williams-Young, D.; Ding, F.; Lipparini, F.; Egidi, F.; Goings, J.; Peng, B.; Petrone, A.; Henderson, T.; Ranasinghe, D.; Zakrzewski, V. G.; Gao, J.; Rega, N.; Zheng, G.; Liang, W.; Hada, M.; Ehara, M.; Toyota, K.; Fukuda, R.; Hasegawa, J.; Ishida, M.; Nakajima, T.; Honda, Y.; Kitao, O.; Nakai, H.; Vreven, T.; Throssell, K.; Mont-

- gomery, J. A., Jr.; Peralta, J. E.; Ogliaro, F.; Bearpark, M. J.; Heyd, J. J.; Brothers, E. N.; Kudin, K. N.; Staroverov, V. N.; Keith, T. A.; Kobayashi, R.; Normand, J.; Raghavachari, K.; Rendell, A. P.; Burant, J. C.; Iyengar, S. S.; Tomasi, J.; Cossi, M.; Millam, J. M.; Klene, M.; Adamo, C.; Cammi, R.; Ochterski, J. W.; Martin, R. L.; Morokuma, K.; Farkas, O.; Foresman, J. B.; Fox, D. J. Gaussian~16 Revision C.01. 2016; Gaussian Inc. Wallingford CT.
- (S5) Rappe, A. K.; Casewit, C. J.; Colwell, K. S.; Goddard, W. A. I.; Skiff, W. M. UFF, a full periodic table force field for molecular mechanics and molecular dynamics simulations. *J. Am. Chem. Soc.* **1992**, *114*, 10024–10035, DOI: 10.1021/ja00051a040.
- (S6) Pye, C. C.; Ziegler, T. An Implementation of the Conductor-like Screening Model of Solvation within the Amsterdam Density Functional Package. *Theor. Chem. Acc.* **1999**, *101*, 396–408, DOI: 10.1007/s002140050457.
- (S7) te Velde, G.; Bickelhaupt, F. M.; Baerends, E. J.; Fonseca Guerra, C.; van Gisbergen, S. J. A.; Snijders, J. G.; Ziegler, T. Chemistry with ADF. *J. Comput. Chem.* **2001**, *22*, 931–967, DOI: 10.1002/jcc.1056.
- (S8) Allinger, N. L.; Zhou, X.; Bergsma, J. Molecular mechanics parameters. *J. Mol. Struct. THEOCHEM* **1994**, *312*, 69–83, DOI: 10.1016/S0166-1280(09)80008-0.
- (S9) van Lenthe, E.; Snijders, J. G.; Baerends, E. J. The zero-order regular approximation for relativistic effects: The effect of spin-orbit coupling in closed shell molecules. *J. Chem. Phys.* **1996**, *105*, 6505–6516, DOI: 10.1063/1.472460.
- (S10) Adamo, C.; Scuseria, G. E.; Barone, V. Accurate excitation energies from time-dependent density functional theory: Assessing the PBE0 model. *J. Chem. Phys.* **1999**, *111*, 2889–2899, DOI: 10.1063/1.479571.
- (S11) Mayer, I. Bond order and valence indices: A personal account. *J. Comput. Chem.* **2007**, *28*, 204–221, DOI: <https://doi.org/10.1002/jcc.20494>.



- (S12) Wiberg, K. B. Application of the pople-santry-segal CNDO method to the cyclopropylcarbiny and cyclobutyl cation and to bicyclobutane. *Tetrahedron* **1968**, *24*, 1083–1096.
- (S13) Van Lenthe, E.; Baerends, E. J. Optimized Slater-type basis sets for the elements 1–118. *J. Comput. Chem.* **2003**, *24*, 1142–1156, DOI: 10.1002/jcc.10255.
- (S14) Reed, A. E.; Weinhold, F. Natural localized molecular orbitals. *J. Chem. Phys.* **1985**, *83*, 1736–1740, DOI: 10.1063/1.449360.
- (S15) Rajapaksha, H.; Mason, S. E.; Forbes, T. Z. Synthesis, Characterization, and Density Functional Theory Investigation of the Solid-State  $[\text{UO}_2\text{Cl}_4(\text{H}_2\text{O})]^{2-}$  Complex. *Inorg. Chem.* **2023**, *62*, 14318–14325, DOI: 10.1021/acs.inorgchem.3c01725.
- (S16) Maintz, S.; Deringer, V. L.; Tchougréeff, A. L.; Dronskowski, R. LOBSTER: A tool to extract chemical bonding from plane-wave based DFT. *J. Comput. Chem.* **2016**, *37*, 1030–1035, DOI: <https://doi.org/10.1002/jcc.24300>.
- (S17) Perdew, J. P.; Chevary, J. A.; Vosko, S. H.; Jackson, K. A.; Pederson, M. R.; Singh, D. J.; Fiolhais, C. Atoms, molecules, solids, and surfaces: Applications of the generalized gradient approximation for exchange and correlation. *Phys. Rev. B* **1992**, *46*, 6671–6687, DOI: 10.1103/PhysRevB.46.6671.
- (S18) Wigner, E. Effects of the electron interaction on the energy levels of electrons in metals. *Trans. Faraday Soc.* **1938**, *34*, 678–685, DOI: 10.1039/TF9383400678.
- (S19) Perdew, J. P.; Burke, K.; Ernzerhof, M. Generalized Gradient Approximation Made Simple. *Phys. Rev. Lett.* **1997**, *78*, 1396–1396, DOI: 10.1103/PhysRevLett.78.1396.
- (S20) Hamprecht, F. A.; Cohen, A. J.; Tozer, D. J.; Handy, N. C. Development and assessment of new exchange-correlation functionals. *J. Chem. Phys.* **1998**, *109*, 6264–6271, DOI: 10.1063/1.477267.

- (S21) Boese, A. D.; Doltsinis, N. L.; Handy, N. C.; Sprik, M. New generalized gradient approximation functionals. *J. Chem. Phys.* **2000**, *112*, 1670–1678, DOI: 10.1063/1.480732.
- (S22) Boese, A. D.; Handy, N. C. A new parametrization of exchange–correlation generalized gradient approximation functionals. *J. Chem. Phys.* **2001**, *114*, 5497–5503, DOI: 10.1063/1.1347371.
- (S23) Wu, Z.; Cohen, R. E. More accurate generalized gradient approximation for solids. *Phys. Rev. B* **2006**, *73*, 235116, DOI: 10.1103/PhysRevB.73.235116.
- (S24) Haas, P.; Tran, F.; Blaha, P.; Schwarz, K. Construction of an optimal GGA functional for molecules and solids. *Phys. Rev. B* **2011**, *83*, 205117, DOI: 10.1103/PhysRevB.83.205117.
- (S25) Schultz, N. E.; Zhao, Y.; Truhlar, D. G. Density Functionals for Inorganometallic and Organometallic Chemistry. *J. Phys. Chem. A* **2005**, *109*, 11127–11143, DOI: 10.1021/jp0539223.
- (S26) Becke, A. D. Density-functional thermochemistry. III. The role of exact exchange. *J. Chem. Phys.* **1993**, *98*, 5648–5652, DOI: 10.1063/1.464913.
- (S27) Stephens, P. J.; Devlin, F. J.; Chabalowski, C. F.; Frisch, M. J. Ab Initio Calculation of Vibrational Absorption and Circular Dichroism Spectra Using Density Functional Force Fields. *J. Chem. Phys.* **1994**, *98*, 11623–11627, DOI: 10.1021/j100096a001.
- (S28) Grimme, S.; Ehrlich, S.; Goerigk, L. Effect of the damping function in dispersion corrected density functional theory. *J. Comput. Chem.* **2011**, *32*, 1456–1465, DOI: 10.1002/jcc.21759.
- (S29) Møller, C.; Plesset, M. S. Note on an Approximation Treatment for Many-Electron Systems. *Phys. Rev.* **1934**, *46*, 618–622, DOI: 10.1103/PhysRev.46.618.

- (S30) Weigend, F.; Ahlrichs, R. Balanced basis sets of split valence, triple zeta valence and quadruple zeta valence quality for H to Rn: Design and assessment of accuracy. *Phys. Chem. Chem. Phys.* **2005**, *7*, 3297–3305, DOI: 10.1039/B508541A.
- (S31) Küchle, W.; Dolg, M.; Stoll, H.; Preuss, H. Energy-adjusted pseudopotentials for the actinides. Parameter sets and test calculations for thorium and thorium monoxide. *J. Chem. Phys.* **1994**, *100*, 7535–7542, DOI: 10.1063/1.466847.
- (S32) Cao, X.; Dolg, M.; Stoll, H. Valence basis sets for relativistic energy-consistent small-core actinide pseudopotentials. *J. Chem. Phys.* **2003**, *118*, 487–496, DOI: 10.1063/1.1521431.
- (S33) Werner, H.-J.; Knowles, P. J.; Knizia, G.; Manby, F. R.; Schütz, M.; Celani, P.; Györffy, W.; Kats, D.; Korona, T.; Lindh, R.; Mitrushenkov, A.; Rauhut, G.; Shamasundar, K. R.; Adler, T. B.; Amos, R. D.; Bennie, S. J.; Bernhardsson, A.; Berning, A.; Cooper, D. L.; Deegan, M. J. O.; Dobbyn, A. J.; Eckert, F.; Goll, E.; Hampel, C.; Hesselmann, A.; Hetzer, G.; Hrenar, T.; Jansen, G.; Köppl, C.; Lee, S. J. R.; Liu, Y.; Lloyd, A. W.; Ma, Q.; Mata, R. A.; May, A. J.; McNicholas, S. J.; Meyer, W.; Miller III, T. F.; Mura, M. E.; Nicklass, A.; O’Neill, D. P.; Palmieri, P.; Peng, D.; Pflüger, K.; Pitzer, R.; Reiher, M.; Shiozaki, T.; Stoll, H.; Stone, A. J.; Tarroni, R.; Thorsteinsson, T.; Wang, M.; Welborn, M. MOLPRO, a package of ab initio programs, version 2023.2.
- (S34) Purvis, I., George D.; Bartlett, R. J. A full coupled-cluster singles and doubles model: The inclusion of disconnected triples. *J. Chem. Phys.* **1982**, *76*, 1910–1918, DOI: 10.1063/1.443164.
- (S35) Fryer-Kanssen, I.; Kerridge, A. Elucidation of the Inverse Trans Influence in Uranyl and Its Imido and Carbene Analogues via Quantum Chemical Simulation. *Chem. Commun.* **2018**, *54*, 9761–9764, DOI: 10.1039/C8CC06088F.